Food Sci. Biotechnol. 21(2): 467-474 (2012)
DOI 10.1007/s10068-012-0059-4

RESEARCH ARTICLE

Rheological Behaviors and Microstructure of Oviductus Ranae Hydrogels

Qing Liang, Shouqin Zhang, and Jinsong Zhang

Received: 13 October 2011 / Revised: 30 December 2011 / Accepted: 20 January 2012 / Published Online: 30 April 2012
© KoSFoST and Springer 2012

Abstract The rheological properties of Oviductus Ranae (OR) hydrogels were systematically investigated with shear viscosity, dynamic oscillation, and creep-recovery measurements. The viscosity curves displayed phenomena of shear thinning with increase of shear rate. The flow behaviors of the hydrogels were described using 2 representative rheological models. The lesser water was absorbed by OR, the higher viscosity and greater extent of thixotropy it presents. Dynamic viscoelasticity measurements indicated that the samples exhibit viscoelastic properties as physical gels. Creep curves also revealed that the hydrogels behave as viscoelastic solids. Damped oscillations were observed in the initial stage of creep tests (0-1 s). The viscoelastic moduli obtained from dynamic oscillations and those from damped oscillations agreed with each other. The strong dependence of rheological behaviour on network of OR hydrogels had been confirmed by electron microscopy.

Keywords: rheological behavior, Oviductus Ranae, hydrogel, viscoelasticity, morphology

Introduction

Oviductus Ranae (OR) is the dry oviductus of the thely-Rana temporaria chensinensis David, which has the characters of uniform caliber, transparence, fat luster, creamy feeling, and special fat smell. It was recorded in Chinese pharmacopoeias from edition 1985 to 2010 as precious and famous Chinese crude drug. With its economic and nutritive value and health-care effect, Oviductus Ranae has broadly applicative potential in foodstuff (e.g., health food), medicine, light industry (e.g., cosmetic), and so on. It could invigorate spleen, stomach, kidney, nourish yin, moisten lung, and promote production of body fluid (1-3), which is attributed to its multiple components. Earlier research suggests that OR is rich in protein, thus it is ideal nutrition protein origin. Meanwhile, there are also abundant polysaccharide, fat, and physiological activators such as estradiol, progestin, and testosterone in OR.

When OR contacts with water, it expands and turns into hydrogels with 3-dimensional cross-linked hydrophilic biopolymer networks that can absorb large quantity of water. Generally, the water accommodated by the hydrogel can be classified as free water, semi-bound water, interstitial water, and bound water (4). Different kinds of water have different cohesion force with biomacromolecules, which drastically increases the expansion index of OR to dozens of times. Consequently, the obtained soft, pliable, degradable OR hydrogels are typical wet materials with a wide range of potential applications in biomedicines, pharmaceutics, food additives, and personal care productions (5-7).

The structure related properties of hydrogel are extremely important in specific applications. Among them, rheological properties study of hydrogels can provide not only important information on their structure (8), but also useful information on the viscoelastic properties as well as the network parameters within the hydrogels, which are imperative for meaningful industrial applications of the hydrogels. Rheology can also be utilized as a practical method to identify the quality of OR, which is usually difficult and inconvenient to be distinguished between actual product and its substitutes/adulterants by other methods like morphological, chemical characteristics (9),

Qing Liang, Shouqin Zhang, Jinsong Zhang (✉)
College of Biological and Agricultural Engineering, Jilin University, Changchun Jilin 130022, China
Tel: +86 431 85562173; Fax: +86 431 85562173
E-mail: jluzjs@jlu.edu.cn

or molecular marker (10).

As compositionally and structurally complex materials, hydrogels exhibit a wide range of rheological properties under different conditions. These properties are strongly affected by temperature, pressure, concentration, and physical state of hydrogels (11-13). To the best of our knowledge, however, there is no report concerning the rheological characteristics of OR hydrogels swelled by different proportions of water. Absence of rheological data is one of the problems encountered during numerical simulation and production design on OR hydrogels. Therefore, our interest of this work was to systematically investigate the rheological properties of Oviductus Ranae (OR) hydrogels, to provide useful information both for basic research and for its potential applications mentioned above. The rheological tests including steady, dynamic, and creep rheological behaviors of OR hydrogels were addressed.

Materials and Methods

Proximate composition and aminoacid analysis of Oviductus Ranae (OR) OR was purchased from Antu Baoli health food Co., Ltd., China and it was produced in Changbai Mountain of Jilin province in Northeast China. The moisture (11.9±0.2%), ash (4.5±0.1%), fat (2.0±0.1%), and crude polysaccharide (13.1±0.1%) contents of OR was determined according to the method as described by AOAC (14,15). The crude protein (62.0±0.1%) content was determined by estimating its total nitrogen content by Kjeldahl method (14). A factor of 5.8 was used to convert the nitrogen value to protein.

Preparation of OR hydrogels The sample of dry OR was ground in porcelain mortar and then sifted through a 40 mesh sieve. Deionized water was used to mix with the powdered OR to form hydrogels. The hydrogels were prepared at 1:60 (OR:water, w/w, sample A), 1:90 (w/w, sample B), 1:120 (w/w, sample C), 1:150 (w/w, sample D), 1:180 (w/w, sample E), and 1:210 (w/w, sample F) concentrations (C_{OR}). All the above 6 samples were allowed to equilibrate for 24 h at room temperature (20°C). In order to remove entrapped air bubbles and acquire homogeneous samples, gentle stirring was imposed on the hydrogel samples. Then they were allowed to equilibrate for another 24 h at 20°C to complete hydrogels structure formation.

Rheological tests All the rheological measurements were performed on a controlled-stress rheometer (AR500; TA Instruments, Fort Sam Houston, TX, USA) and equipped with an aluminum parallel plate geometry (diameter= 40 mm, gap size setting=1 mm). Each kind of rheological experiment was performed at its corresponding temperature, and the temperature was controlled by a water bath connected to the Peltier system in the bottom plate. A thin layer of silicone oil was applied on the surface of the samples in order to prevent evaporation. The linear viscoelastic (LVE) region was determined for each sample through a frequency strain-sweep measurement at 1 Hz (data not shown). Viscoelastic properties of OR hydrogel samples were determined within the linear viscoelatic region. An equilibration of 3 min was performed before each measurement.

***Continuous shear measurements*:** The continuous shear tests were performed at 20°C over the shear rate range of 0.001-2,000 1/s to measure the apparent viscosity. In order to perform a quantitative comparison and examination of OR hydrogel samples, 2 rheological flow models based on shear rate-apparent viscosity were used to examine the flow behavior of the samples:

Herschel-Bulkley (H-B) model

$$\sigma = \sigma_0 + K\dot{\gamma}^n \quad (1)$$

Carreau model

$$\eta = \eta_\infty + (\eta_0 - \eta_\infty) \times [1 + (\lambda\dot{\gamma})^2]^{(n-1)/2} \quad (2)$$

where, σ_0 is yield stress, K is the consistency index, and n is the flow behavior index, η_0 and η_∞ are the asymptotic values of viscosity at zero-shear rate and infinite shear rate, respectively, λ is a time constant with the dimensions of time.

***Determination of thixotropic properties*:** Shear stress-shear rate (flow curves) data were obtained at 20°C on the samples. The instrument was programmed for set temperature and equilibration followed by 2-cycle shear in which the shear rate was increased linearly from 0 to 100 1/s in 3 min (up curve) and immediately decreased from 100 to 0 1/s in the next 3 min (down curve). This process was repeated 2 more times for each sample. Data from the ascending and descending segments of the shear cycle were used to characterize the flow of the samples and to estimate the power-law parameters by using the equation:

$$\sigma = K\dot{\gamma}^n \quad (3)$$

where, K is the consistency index (Pa s^n), and n is the flow behavior index.

***Oscillatory rheological properties*:** Small amplitude oscillatory tests were performed at 20°C over the frequency range of 0.1-100 rad/s. The strain amplitude for the frequency sweep measurements was selected as 1%, which was in the linear viscoelastic region for all samples. The mechanical spectra were obtained through recording storage modulus (G'), loss modulus (G''), and loss tangent ($\tan\delta = G''/G'$) as function of angular frequency.

***Creep-recovery measurements*:** Creep-recovery experiments

were carried out using shear stress of 7.958 Pa at 20°C. The variation in shear strain in response to the applied stress was measured over a period of 3 min; the stress was then removed, and changes in strain were recorded for a further period of 3 min.

Morphology observation SEM (JSM 6700-F; Jeol, Tokyo, Japan) was used to evaluate the microstructure of the gels formed. The OR hydrogels were freeze-dried and the freeze-dried gel specimens were hand-fractured and the fracture surface was coated with gold. The morphology of the freeze-dried samples were observed using a scanning electron microscope (JSM 6700-F; Jeol) at 5.0 kV.

Statistical analysis The experimental results obtained from this study were fitted to different kinetic and mathematical model using TA Rheology Advantage Data Analysis software V 5.4.7 (TA Instruments). The fit and estimates were calculated at a significance level of 95%. The best fit regression model could be selected on the basis of standard error (SE), which is defined as:

$$\frac{\Sigma(X_m - X_c)^2/(n-2)^{0.5}}{Range} \times 1000 \quad (4)$$

where, X_m is the measured value; X_c is the calculated value, n is the number of data points and *range* is the difference between the maximum value of X_m and the minimum value.

Results and Discussion

Steady flow behavior measurements and yield stress measurements The viscosity curves (apparent viscosity ($\eta_{app} = \sigma/\dot{\gamma}$) vs. shear rate) of OR with various mass concentrations at 20°C are shown in Fig. 1. They show infrequent characteristics for hydrogels: in the region of low shear rate (less than 0.04 1/s), the samples present 'shear thickening'; and with the increase of shear rate, the apparent viscosity reaches a maximum, then decreases at higher shear rates which is termed as shear thinning phenomenon. The relationship between η_{app} and C_{OR} is valuable for setting guidelines for estimating the rheological behavior of formulated products containing OR hydrogels. It is difficult to capture all possible trends of flow behavior using a single rheological model. Therefore 2 rheological models were used in the present study as H-B model and Carreau model. The H-B model is able to estimate yield stress. And the Carreau model is able to calculate viscosity at a theoretically zero shear rate (η_0) and infinite shear rate (η_∞). The parameters of different rheological models obtained from regression analysis are summarized in Table 1.

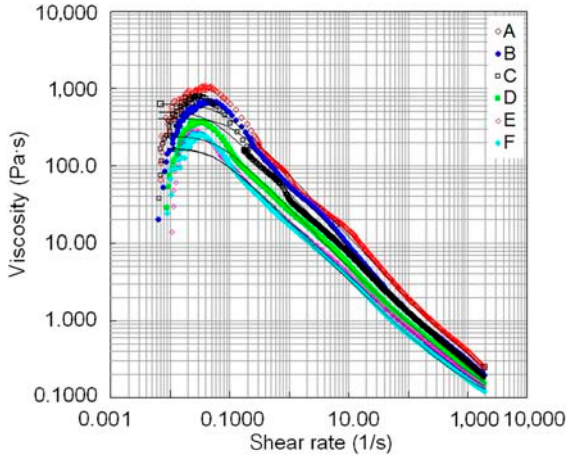

Fig. 1. Viscosity curves for Oviductus Ranae hydrogels. The predicted results based on Carreau model are shown with solid lines.

Table 1. Comparison of different models for the flow behavior of Oviductus Ranae hydrogels with various mass concentrations

Sample	Model	σ_0[1)] (Pa)	K (Pa·s^n)	n	η_0 (Pa·s)	η_∞ (Pa·s)	λ (s)	SE
A	Herschel-Bulkley	5.220 (51.31)	61.12	0.2598	NA	NA	NA	30.30
	Carreau	NA	NA	0.7963	623.7	0.06825	14.29	34.43
B	Herschel-Bulkley	22.39 (26.46)	25.44	0.3393	NA	NA	NA	33.47
	Carreau	NA	NA	0.8458	410.4	0.1175	9.717	36.05
C	Herschel-Bulkley	12.76 (17.22)	25.26	0.3397	NA	NA	NA	16.93
	Carreau	NA	NA	0.7902	498.4	0.09471	21.64	30.54
D	Herschel-Bulkley	9.568 (16.88)	15.07	0.3812	NA	NA	NA	15.41
	Carreau	NA	NA	0.7531	241.5	0.06589	17.55	25.92
E	Herschel-Bulkley	5.277 (9.935)	12.46	0.3932	NA	NA	NA	9.76
	Carreau	NA	NA	0.7128	165.5	0.05231	19.94	31.71
F	Herschel-Bulkley	7.896 (8.960)	8.226	0.4318	NA	NA	NA	13.77
	Carreau	NA	NA	0.7442	168.7	0.06384	19.83	26.33

[1)]Numbers in the brackets stand for yield stress obtained from the curve of apparent viscosity against shear stress (figure not shown).

As can be seen from Table 1, the rheological data for the OR hydrogels can be adequately described using the 2 above models. And they generally give low SE and show good fit for data points under most other circumstances (16-18). The yield stress (σ_0) represents a finite stress required to initiate flow. The σ_0 values of the samples determined by H-B model do not show any trend with C_{OR} (see Table 1, the yield stress of sample A is unexpectedly the smallest among all the tested samples) suggesting that these calculated values can only be considered as model fitting parameters not true σ_0 of the samples. From the curve of apparent viscosity against shear stress (figure not shown) the realistic σ_0 values can be gained and these values of yield stress are also showed in Table 1 (in brackets). As C_{OR} decreased from 1:60 to 1:210, the interaction between hydrogel molecules which restricts molecular motion decreased, hence σ_0 decreases. Increasing OR concentration decreased the flow behavior index n (relates to the higher viscosity of OR hydrogel corresponds to a higher degree of pseudoplastic properties) and increased the consistency coefficient K (relates to the increase of water binding capacity), which are in agreement with the section of thixotropic properties below.

The fits to the experimental data, using the Carreau model, are also shown in Table 1 (reported as solid lines in Fig. 1, the H-B model is not shown). Calculated zero shear rate viscosities η_0 have obvious concentration dependence, and there is large deviation between calculated and real values, which also shows that the η_0 can only be considered as a model fitting parameter. The rate index n does not decrease noticeably with C_{OR}, and this indicates that the samples have similar shear thinning properties.

The apparent viscosities of all the samples decreased with increasing shear rate (larger than 0.04 1/s), which shows that all the samples have shear-thinning behaviors. The fact indicates that higher concentration results in higher η_{app} in the tested shear rate range, and this is consistent with what was found earlier (13,19). This is probably because protein and polysaccharide molecules entangle by overlapping and interpenetrating into each other at higher C_{OR}. This limits the water penetration and restricts the fluidity of hydrogels. Consequently, higher η_{app} was always observed at higher C_{OR}. With the increase of shear rate, there will be disentanglement of long chain molecules which leads to the reduction of intermolecular resistance to flow. There is no Newtonian region at high shear rates, thus the samples are not capable of maintaining part of its initial overall structure (20).

Although there is a qualitatively good agreement between experiment and the models, a deviation between the model and the experimental data at low shear rates can be observed (less than 0.04 1/s, Fig. 1). They all have a similar character that an initial 'shear-thickening' behavior was observed, where the apparent viscosity increases with increasing shear rate and reaches a maximum value. In principle, there is no real shear thickening flow behavior. Because of interactions among those biomacromolecules, at low shear rate the applied stress is distributed over the entire hydrogel specimens and therefore, each bond (hydrogen or ionic bond) sustains this energy by deforming to a large strain. The slow effect of shear makes the bonds to stretch to their full capacity before starting to fail, which means the course of shear thinning begins.

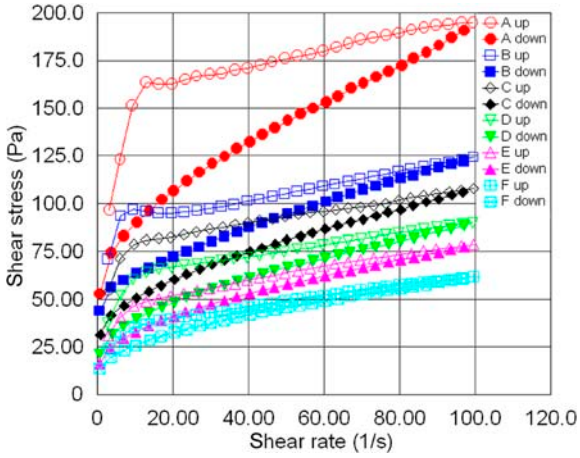

Fig. 2. Thixotropy loop for Oviductus Ranae hydrogels.

Determination of thixotropic properties The thixotropy of OR hydrogels of various mass concentrations are presented in Fig. 2. For the range of shear rates used in this study, the power-law model describes flow behavior of each sample. Consistency coefficients (K) and flow behavior indices (n) along with coefficients of determination (R^2) as influences of OR concentrations for each flow curve are shown in Table 2. From Table 2, a much bigger value of K can be observed in the up flow curve than that in the down flow curve, indicating a more significant thinning effect, in agreement with the thixotropic behavior of the samples. Besides, the n value of the up curve is smaller than the corresponding value of the down curve, indicating an increase in plasticity of the new-formed structures. Appearance of a hysteresis area in the plot of shear stress vs. shear rate means that all hydrogels exhibit time-dependent behavior.

All the samples exhibit clockwise hysteresis loop, indicating that shear stress obtained from the increasing-order of shear rate (up curve) is much larger than the corresponding value of the decreasing-order of shear rate (down curve), which suggests thixotropic behavior of the hydrogels. At low shear rate of up curve of shear stress, samples A and B increase quickly with increase of shear rate. So the hydrogels exhibited extremely thixotropic behavior, which manifests as a regional peak in the

Table 2. Power law parameters and coefficients of thixotropic breakdown for Oviductus Ranae hydrogels

Sample	K_d	Up curve			Down curve		
		K (Pa · s^n)	n	R^2	K (Pa · s^n)	n	R^2
A	0.2096±0.009[1)]	102.70±2.85	0.1406±0.003	0.949	41.63±1.43	0.3216±0.006	0.990
B	0.1402±0.006	65.50±1.45	0.1291±0.006	0.937	33.29±0.47	0.2737±0.004	0.978
C	0.1635±0.012	51.86±0.85	0.1536±0.005	0.981	23.96±0.06	0.3164±0.006	0.990
D	0.1546±0.005	36.40±2.05	0.1920±0.005	0.981	17.38±0.11	0.3477±0.005	0.994
E	0.1266±0.014	24.56±1.73	0.2456±0.011	0.994	13.52±0.06	0.3753±0.008	0.996
F	0.1127±0.013	18.06±0.73	0.2624±0.013	0.994	10.72±0.04	0.3470±0.011	0.996

[1)]Value represent the mean±SD (n=3); Value significance level α=0.05

ascending curve of hysteresis loop. The clockwise loops can be interpreted as structure breakdown by the shear field (thixotropic behavior) to alter a structure or form a new structure. The magnitude of the hydrogels thixotropy could also be estimated as the coefficient of thixotropic breakdown, K_d, which is defined as the ratio of the hysteresis area to the area beneath the ascending shear curve (16):

$$K_d = \frac{A_{up} - A_{down}}{A_{up}} \quad (5)$$

where, A_{up} and A_{down} are the areas under ascending and descending flow curves, respectively.

Coefficient of thixotropic breakdown shows decreasing tendency with decrease of C_{OR} (see the column of K_d). Since a coefficient of thixotropic breakdown is an index of the energy needed to destroy the structure of the system, the experimental data indicate that high C_{OR} hydrogels need higher energy to breakdown the structure. That increase in K_d, as well as in apparent viscosity, is due to entanglement of further more molecules of proteins and polysaccharides and results in tight packing of the macromolecules mentioned above.

Oscillatory rheological properties Oscillatory (dynamic) rheological properties were used along with flow tests to provide insight on the structure of the samples (21). Dynamic frequency sweep tests were performed in the linear viscoelastic range to determine the frequency dependence of the storage modulus (G') and loss modulus (G'') (22). As can be seen from Fig. 3, the elastic modulus curve is higher than that of G'' over the frequency range analyzed. In particular, from the mechanical spectra, it is possible to distinguish between chemical (strong) gel and physical (weak) gels. The principle differences between chemical and physical gels lie in the lifetime and the functionality of the network functions. In the case of a physical gel, the profile of G' and G'' moduli show slight frequency dependence and the ratio G''/G' is higher than 0.1 (the same as Fig. 3). As expected, tan δ is found to be

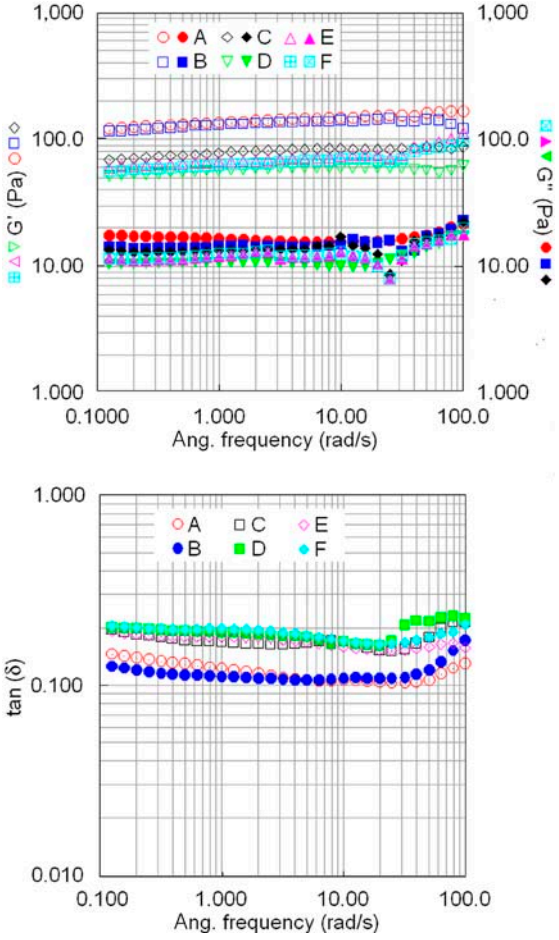

Fig. 3. Frequency dependence of the Oviductus Ranae hydrogels.

practically independent of frequency for all samples, indicating that the system has transformed with respect to the viscoelastic solid state. Such rheological behavior (the predominance of elasticity rather than viscosity in hydrogels) is typical of biological gels such as protein and polysaccharide based networks and soft tissues. So OR hydrogels can be defined as physical (weak) gels. In physical gels, cross-links are formed by non-covalent bonds such as hydrophobic interaction and hydrogen bonding. Indeed, they are essentially strain independent of

deformations of lower than 0.2-0.3, whereas the linear viscoelastic region may extend to large strains.

Creep-recovery measurements The creep-recovery behaviors of the samples exhibit a typical viscoelastic behavior (figure not shown) similar to that of agar/κ-carrageenan mixtures (23). The strain values increase almost linearly with time after sometime (e.g., 80 s for the sample F) of testing, suggesting that the deformation after this time is mainly due to the viscous flow. With the decrease of concentration, the time of change becomes longer. So for the samples A, B, and C the creep phase is relatively flat and close to horizontal (compared with other samples) and there is an instantaneous elastic response followed by a constant compliance during recovery period. It has been accepted that the stronger sample with greater resistance to deformation had smaller creep strain than the softer one. Among the 6 groups of curves, sample A exhibits smallest creep strain and sample F exhibits the biggest creep strain and the other samples behave between them. The recovery (%) was used to identify the recovery percentage of the samples. The higher the recovery phase, the higher is the viscoelastic solid character of the sample. The recovery rate was defined as following:

$$\text{Recovery}=\frac{\text{maximum strain}-\text{finished strain}}{\text{maximum strain}} \quad (6)$$

Calculation shows that all the samples exhibit similar strain recovery after the removal of load (about 80%, A 82.61%, B 78.82%, C 87.80%, D 83.46%, E 76.44%, and F 79.50%), indicating that the samples had similar elastic properties. The fact also indicates that OR hydrogels have unique properties: although changes in mass concentration from 1:60 to 1:210 seem quite large, they can keep their own nearly unchanged viscoelastic solid characteristics.

In the start of a creep test, if the tested sample is sufficiently viscoelastic, damped oscillations (creep ringing) are observed in the angular displacement measured. In creep-recovery measurements, the similar phenomena appeared (Fig. 4). Though these inertial effects are often undesirable, they can be exploited to slightly extend the accessible range of oscillatory measurements. The data extracted can also be compared with that measured in dynamic oscillatory rheological tests (forced oscillations) in order to check for self-consistency (24). Figure 4 shows data from a creep test on the sample A (the curves of other samples are not shown here). The creep strain behavior, $\gamma(t)$, of whole sample was fitted using the following expression for Jeffreys strain (Eq. 7) and Voigt strain (Eq. 10). The reason why these 2 constitutive models were chosen is they are applied widely. The Jeffreys model shows a steady rate of creep as expected in a viscoelastic fluid, and the Voigt model is the canonical model for a viscoelastic solid (24) .

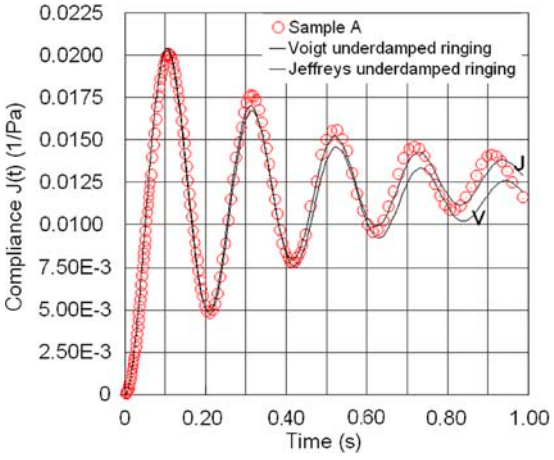

Fig. 4. Inertio-elastic ringing fit to both Voigt and Jeffreys model in the creep mode for an Oviductus Ranae hydrogel (sample A).

Jeffreys model

$$\gamma(t)=\dot{\gamma}_J t-B_J-e^{-A_J t}\left[B_J\cos(\omega_J t)+\frac{A_J}{\omega_J}\left(B_J-\frac{\dot{\gamma}_J}{A_J}\right)\sin(\omega_J t)\right] \quad (7)$$

$$G'=G_J\frac{(\lambda_2\omega)^2}{1+(\lambda_2\omega)^2} \qquad G''=G_J\frac{(\lambda_2\omega)[1+(\lambda_1^2-\lambda_1\lambda_2)\omega^2]}{1+(\lambda_1\omega)^2} \quad (8)$$

$$\lambda_1=(\eta_1+\eta_2)/G_J \qquad \lambda_2=\eta_2/G_J \quad (9)$$

Voigt model

$$\gamma(\tau)=\gamma_K\left\{1-e^{-A_K t}\left[\cos(\omega_K t)+\frac{A_K}{\omega_K}\sin(\omega_K t)\right]\right\} \quad (10)$$

$$G'=G_K \qquad G''=\eta_K\omega \quad (11)$$

The damped oscillatory response for the 2-parameter Voigt model and 3-parameter Jeffreys model were fitted to the experimental data using computer software (Rheology Advantage Data Analysis; TA Instruments, data not shown here). When the model parameters were determined, we manually converted the fitted model parameters to the viscoelastic moduli G' (ω_*), G'' (ω_*), and tan δ (Table 3) using the equation of 8, 9, and 11. Compared with the results of forced oscillations, the values of G' (ω_*) and G'' (ω_*) have relatively good consistency with G' and G'', though there is a deviation between them. But these kinds of experimental errors do not influence the characterization of viscoelastic features from which the same conclusions as dynamic rheological experiment can be drawn.

Morphology Typical cross-sectional SEM images of freeze-dried OR gel prepared from sample A and sample E

Table 3. Comparison of the viscoelastic moduli of dynamic oscillatory measurements and those determined from inertio-elastic creep ringing by fitting 2 assumed constitutive models: Jeffreys and Voigt

Sample and Model	ω (ω_*)[1)] (rad/s)	$G'(\omega)$ $G'(\omega_*)$ (Pa)	$G''(\omega)$ $G''(\omega_*)$ (Pa)	tan δ
Sample A	30.66	96.08	12.16	0.127
Jeffreys	28.86	87.92	13.25	0.151
Voigt	27.64	86.49	13.46	0.156
Sample B	25.54	58.46	8.48	0.145
Jeffreys	23.09	59.54	9.14	0.153
Voigt	22.30	58.35	8.84	0.152
Sample C	23.93	52.62	7.65	0.145
Jeffreys	22.05	55.45	10.89	0.196
Voigt	21.57	53.95	10.76	0.199
Sample D	20.22	38.91	6.49	0.167
Jeffreys	17.21	37.71	8.23	0.218
Voigt	16.92	35.42	9.10	0.257
Sample E	21.81	47.46	8.56	0.180
Jeffreys	16.08	42.35	9.46	0.223
Voigt	16.77	38.00	12.34	0.326
Sample F	18.51	34.22	8.43	0.246
Jeffreys	14.65	29.94	8.95	0.299
Voigt	13.63	27.84	8.48	0.305

[1)]Letter of ω_* stands for the values of Jeffreys or Voigt models.

were depicted in Fig. 5. Apparently, both gels had comparable highly porous interior structures with the pores interconnected, suggesting high water retention capacity. The density of the gel network was proportionally related to the concentration of biomacromolecules. Protein/polysaccharide gels are generally characterized as fine networks of biomacromolecule aggregates. With the concentration going from low to high, the pore structures of the resulting gels dramatically change from macroporous to microporous, giving more compact porous structure and smaller pore size. Along with this change, the density of the biomacromolecule network increases accordingly. This is mainly explained by the entanglings between biomacromolecules and crosslinking densities being enhanced with the increase of OR content. The structural characteristics mentioned above determine the rheological properties of OR hydrogels, for instance, high-density (high-strength) network leads to high appearent viscosity and yield stress. The rheological parameters, meanwhile, also further proof that the net structure of OR hydrogels exhibit extremely shear-thinning and thixotropic behavior: when shear stress act on the gel samples, their net structures are destroyed (shear thinning) and then can be restored to the original state some time later (thixotropy). The unique gel networks are also a guarantee of their satisfactory viscoelasticity. Our test showed OR hydrogel network can

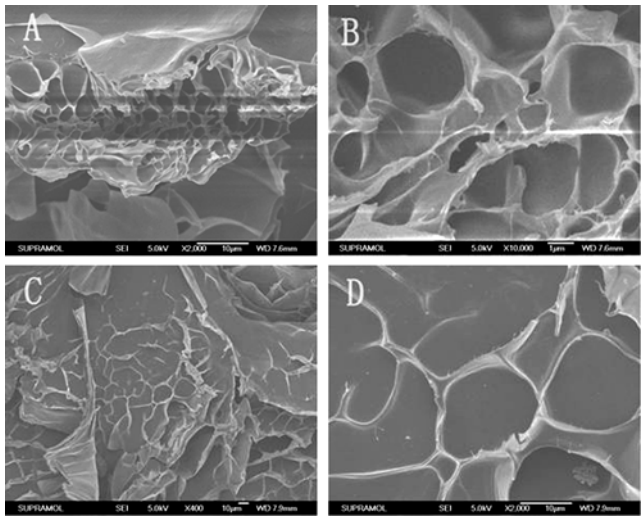

Fig. 5. SEM micrographs taken at the break surface of the Oviductus Ranae hydrogels. Magnitude (A, Sample A) ×2,000; (B, Sample A) ×10,000; (C, Sample E) ×400; (D, Sample E) ×2,000

be formed in a wide concentration range, meaning that it has great potential capacities as water holding, gelation, and thickening materials.

Acknowledgments This work was financially supported by the Fundamental Research Funds for the Central Universities.

References

1. Liu Y, Liu LX. Ingredient and pharmacology research progress of Oviductus Ranae. Strait Pharm. J. 19: 1-3 (2007)
2. Hu X, Liu CB, Chen XP, Wang LM. Main nourishment components of Oviductus ranae. J. Jilin Agr. Univ. 25: 218-220 (2003)
3. Liang L, Zhang XH, Zhou Y, Huang YJ, Deng HZ. Protective effect of Oviductus Ranae capsules on the reproductive organs of aged mice. J. Southern Med. Uni. 28: 982-985 (2008)
4. Omidian H, Park K. Introduction to hydrogels. pp. 1-16. In: Biomedical Applications of Hydrogels Handbook. Ottenbrite RM, Park K, Okano T (eds). Springer, New York, NY, USA (2010)
5. Beebe DJ, Moore JS, Bauer JM, Yu Q, Liu RH, Devadoss C, Jo BH. Functional hydrogel structures for autonomous flow control inside microfluidic channels. Nature 404: 588-590 (2000)
6. Kulicke WM, Eidam D, Kath F, Kix M, Kull AH. Hydrocolloids and rheology: Regulation of viscoelastic characteristics of waxy rice starch in mixture with galactomannans. Starch-Starke 48: 105-114 (1996)
7. Dill KA. Strengthening biomedicine's roots. Nature 400: 309-310 (1999)
8. Saxena A, Kaloti M, Bohidar HB. Rheological properties of binary and ternary protein-polysaccharide co-hydrogels and comparative release kinetics of salbutamol sulphate from their matrices. Int. J. Biol. Macromol. 48: 263-270 (2011)
9. He BZ, Xie LS. On the identification of Oviductus Ranae it's adulterant by water test. Bull. Chin. Mater. Med. 12: 583-585 (1987)
10. Yang XG, Wang YQ, Zhou KY, Liu ZQ. Authentication of Oviductus Ranae and its original animals using molecular marker. Biol. Pharm. Bull. 25: 1035-1039 (2002)
11. Olayide S, Lawal JS, Henning S, Derek L, Dieter L, Kulicke WM.

Hydrogels based on carboxymethyl cassava starch cross-linked with dior polyfunctional carboxylic acids: Synthesis, water absorbent behavior, and rheological characterizations. Eur. Polym. J. 45: 3399-3408 (2009)
12. Mourtasa S, Haikoua M, Theodoropoulloua M, Tsakirogloub C, Antimisiaris SG. The effect of added liposomes on the rheological properties of a hydrogel: A systematic study. J. Colloid Interf. Sci. 317: 611-619 (2008)
13. Laia GL, Lia Y, Li GY. Effect of concentration and temperature on the rheological behavior of collagen solution. Int. J. Biol. Macromol. 42: 285-291 (2008)
14. AOAC. Official Methods of Analysis of AOAC. Method 920.153, 950.46, 960.39, 992.15. Association of Official Analytical Chemists, Washington, DC, USA (1990)
15. Dubois M, Gilles KA, Hamilton JK, Rebers PA, Smith F. Colorimetric method for determination of sugars and related substances. Anal. Chem. 28: 350-356 (1956)
16. Dokić L, Dapčević T, Krstonošić V, Dokić P, Hadnađev M. Rheological characterization of corn starch isolated by alkali method. Food Hydrocolloid. 24: 172-177 (2010)
17. Jung WJ, Han JA, Lim ST. Thermal and rheological properties of hydrogels prepared with retrograded waxy rice starch powders. Food Sci. Biotechnol. 19: 1649-1654 (2010)
18. Khounvilay K, Sittikijyothin W. Rheological behaviour of tamarind seed gum in aqueous solutions. Food Hydrocolloid. 26: 334-338 (2012)
19. Moraes ICF, Carvalho RA, Bittante AMQB, Solorza-Feria J, Sobral PJA. Film forming solutions based on gelatin and poly(vinyl alcohol) blends: Thermal and rheological characterizations. J. Food Eng. 95: 588-596 (2009)
20. Hassan N, Messina PV, Dodero VI, Ruso JM. Rheological properties of ovalbumin hydrogels as affected by surfactants addition. Int. J. Biol. Macromol. 48: 495-500 (2011)
21. Choi YH, Lim ST, Yoo B. Measurement of dynamic rheology during ageing of gelatine-sugar composites. Int. J. Food Sci. Tech. 39: 935-945 (2004)
22. Basu S, Shivhare US, Singh TV, Beniwal VS. Rheological, textural, and spectral characteristics of sorbitol substituted mango jam. J. Food Eng. 105: 503-512 (2011)
23. Norziah MH, Foo SL, Karim AA. Rheological studies on mixtures of agar (*Gracilaria changii*) and κ-carrageenan. Food Hydrocolloid. 20: 204-217 (2006)
24. Ewoldt RH, McKinley GH. Creep ringing in rheometry or how to deal with oft-discarded data in step stress tests! Rheol. Bull. 76: 22-24 (2007)